Inorganica Chimica Acta, *139* (1987) 223–241

Spectroscopic Properties of Tetravalent Actinide Ions in Solids*

J. C. KRUPA

Laboratoire de Radiochimie, Institut de Physique Nucléaire, B.P. 1, 91406 Orsay, France

Abstract

Optical spectroscopy is a powerful tool to study the electronic structure of an optically active transition ion in the condensed phase media and consequently to study the interactions between the central ion and its environment. Up to now a great deal of effort has been made in interpreting the energy levels of the 3+ actinide (An) ions diluted in different single crystal matrices using the successful parametric approach developed for the 3+ lanthanides (Ln). The emphasis on An^{4+} is more recent and is partly due to the development of new host materials such as $ThBr_4$, $ThCl_4$ and the already known $ThSiO_4$, that are characterized by a rather weak crystal-field strength which makes possible the use of the same theoretical approach as for Ln^{3+}. Following this parametric model, the main interactions that are essential for an understanding of the energy level distribution of an f^n ion in solids are briefly examined and the deduced free-ion and crystal-field parameters for Pa^{4+}, U^{4+} and Np^{4+} are compared to those of the lanthanide ions with isoelectronic configuration.

Finally, the actinide series offers an interesting situation since the 5f electrons in the metals are delocalized in the light actinides and localized in the heavy actinides, which could affect the nature of the chemical bonding in the two parts of the series. Is this trend reflected in the An^{4+} spectroscopic parameters?

Introduction

The most important feature that characterizes the lanthanide (Ln) and actinide (An) elements is the small spatial extension of the open f shell which is under completion and contains the optically active electrons. If these elements are engaged in compounds, the f electrons which belong to inner orbitals are well protected from the ligand interactions by the closed ns^2np^6 external orbitals ($n = 5$ for lanthanides (4f) and $n = 6$ for actinides (5f)). Accordingly, the f electrons interact weakly with the electrons of neighbouring atoms and the electronic properties are only slightly affected by the environment. In particular, the solid state spectra of the 4f and 5f ions retain more or less their atomic character, which is of great help in interpreting their level structure. In turn the small perturbation can be used to investigate the surrounding of the ion which then acts as a local probe.

However, some differences exist between the two series. The 4f electrons are well localized and can be considered as core electrons with a small influence upon the binding, which explains the dominant 3+ oxidation state in the lanthanide series. In contrast, in the early actinides: Pa, U, Np, Pu and Am, the 5f orbitals tend to have a greater extension and consequently the contribution of the delocalized 5f electrons to the bonding is increased. The delocalization gives rise to a large variety of oxidation states leading to a large number of possible lowest electronic configurations (Table I) which is a characteristic of the first half of the actinide series. As the atomic number Z increases, the nuclear attraction stabilizes the 5f orbitals and the 5f electrons become more and more localized with a reduction of their bonding ability. From this point of view, the 5f electrons can be considered as an intermediate case between the 4f localized electrons and the 3d 'extended' electrons which are very sensitive to their ligand environment.

A large fraction of our knowledge of the electronic states in solids has been obtained by optical spectroscopy and many important developments come from studies of the rare earth ions Ln^{3+} embedded in crystalline hosts (LaX_3, X = F, Cl, Br) [1, 2]. In the crystal, the metallic ion gives up the field-free spherical symmetry and comes under the influence of the inhomogeneous electrostatic field generated by the electrical charge distribution of the ligands. The crystal-field interaction removes the degeneracy of the J states of the free-ion into a number of M_J crystal-field levels depending upon the symmetry of the environment which is the symmetry of the site occupied by the ion.

Knowledge of the symmetry of the crystal field is very helpful in interpreting ion optical spectra. Through the group theory concepts based on symmetry properties [3], the crystal-field levels are asso-

*Paper presented at the Second International Conference on the Basic and Applied Chemistry of f-Transition (Lanthanide and Actinide) and Related Elements (2nd ICLA), Lisbon, Portugal, April 6–10, 1987.

0020-1693/87/$3.50

TABLE I. Lowest Electronic Configurations of An^0, An^{3+}, An^{4+} and Ln^{3+} with *LSJ* Ground State

Z	Element	Electronic configurations				Element	Z
		An^0	An^{3+}	An^{4+}	Ln^{3+}		
90	Th	$6d^2\,7s^2$	$5f^1\,(^2F_{5/2})$		$4f^1\,(^2F_{5/2})$	Ce	58
91	Pa	$5f^2\,6d\,7s^2$	$5f^2\,(^3H_4)$	$5f^1\,(^2F_{5/2})$	$4f^2\,(^3H_4)$	Pr	59
92	U	$5f^3\,6d\,7s^2$	$5f^3\,(^4I_{9/2})$	$5f^2\,(^3H_4)$	$4f^3(^4I_{9/2})$	Nd	60
93	Np	$5f^4\,6d\,7s^2$	$5f^4\,(^5I_4)$	$5f^3\,(^4I_{9/2})$	$4f^4\,(^5I_4)$	Pm	61
94	Pu	$5f^6\,7s^2$	$5f^5\,(^6H_{5/2})$	$5f^4\,(^5I_4)$	$4f^5\,(^6H_{5/2})$	Sm	62
95	Am	$5f^7\,7s^2$	$5f^6\,(^7F_0)$	$5f^5\,(^6H_{5/2})$	$4f^6\,(^7F_0)$	Eu	63
96	Cm	$5f^7\,6d\,7s^2$	$5f^7\,(^8S_{7/2})$	$5f^6\,(^7F_0)$	$4f^7\,(^8S_{7/2})$	Gd	64
97	Bk	$5f^8\,6d\,7s^2$	$5f^8\,(^7F_6)$	$5f^7\,(^8S_{7/2})$	$4f^8\,(^7F_6)$	Tb	65
98	Cf	$5f^{10}\,7s^2$	$5f^9\,(^6H_{15/2})$	$5f^8\,(^7F_6)$	$4f^9\,(^6H_{15/2})$	Dy	66
99	Es	$5f^{11}\,7s^2$	$5f^{10}\,(^5I_8)$	$5f^9\,(^6H_{15/2})$	$4f^{10}\,(^5I_8)$	Ho	67
100	Fm	$5f^{12}\,7s^2$	$5f^{11}\,(^4I_{15/2})$	$5f^{10}\,(^5I_8)$	$4f^{11}\,(^4I_{15/2})$	Er	68
101	Md	$5f^{13}\,7s^2$	$5f^{12}\,(^3H_6)$	$5f^{11}\,(^4I_{15/2})$	$4f^{12}\,(^3H_6)$	Tm	69
102	No	$5f^{14}\,7s^2$	$5f^{13}\,(^2F_{7/2})$	$5f^{12}\,(^3H_6)$	$4f^{13}\,(^2F_{7/2})$	Yb	70
103	Lr	$5f^{14}\,6d\,7s^2$	$5f^{14}\,(^1S_0)$	$5f^{13}\,(^2F_{7/2})$	$4f^{14}\,(^1S_0)$	Lu	71

ciated with irreducible representations (Γ_n) belonging to the symmetry group under consideration. In addition to the number and degeneracy of crystal-field levels coming from each J level of the free-ion, the group theory methods permit one to establish the selection rules which govern the transitions between these levels. With respect to the polarization properties of the light and the crystal orientation, the optical spectra reveal the nature and the multipolarity of the transitions (the dipolar electric transitions are the most intense unless an inversion centre exists as a symmetry element of the group).

For Ln^{3+}, An^{3+} and An^{4+}, the lowest electronic configurations due to the lone non-closed f-shell are respectively $4f^n$ and $5f^n$ ($1 \leqslant n \leqslant 14$). Then, most of the observed transitions in the optical spectroscopy energy range occur between crystal-field levels within f^n configurations. They are rather weak and sharp. This is a consequence of the Laporte selection rules stating that the electric dipole transitions between two states of the same parity are forbidden. Therefore the observed zero-phonon transitions in a non-centrosymmetric lattice site are forced electric dipole transitions (an inversion centre causes the matrix element $\langle u|P|u'\rangle$ to be zero). This means that the f wavefunctions are not pure and contain a contribution from excited opposite parity configurations. However, this admixture, achieved through the odd terms of the Hamiltonian describing the crystal-field interaction, is small enough to preserve the f character of the levels. Because of the decrease in configuration spacings due to the greater extension of the 5f orbitals, the configuration interactions which mix wavefunctions with the same L and S is more pronounced in actinides than in lanthanides and the effect is expected to be more important for tripositive than for tetrapositive actinide ions.

A great deal of effort had been made in interpreting the spectra of the trivalent lanthanides [4–7] and the corresponding actinides [8–11] in lanthanum halide crystals especially. But as the actinide series offers an interesting situation due to the various oxidation states of the ions, the extension of the previous work was of great interest to test the crystal-field model validity through the series for different ion charges and crystal-field strengths.

To explore the systematic trends, one needs crystalline hosts which on the one hand are optically inactive in the investigated energy range, and on the other hand stabilize the selected oxidation state of the ion. Moreover, the radii of the mutually substituted ions should be of the same size to avoid site distortions. In addition, the site symmetry should be high enough to facilitate the interpretation of the energy levels with the help of the selection rules. The development of new host materials offering these qualities, such as $ThBr_4$ and $ThCl_4$ [12], gave a new impulse to An^{4+} spectroscopy, unfortunately limited by the reducing properties of the melt during the crystal growth. $ThSiO_4$ seems more promising.

Optical spectra of the f ions in the solid state very often contain many more lines than expected from the splitting of the free ion J levels. Apart from the extra lines due to impurities and crystal lattice defects which change the site symmetry, some transitions called vibronics are generated by the coupling of electronic transitions with the vibration modes of the lattice. They are usually weaker and broader and they obey different selection rules according to the space group representation. Temperature experiments are helpful in revealing the vibronic nature of these transitions, especially for local symmetries showing an inversion centre.

TABLE II. Degeneracy of f^n Configurations

Configurations	Terms ^{2S+1}L				Number of J levels $^{2S+1}L_J$	Maximum number of crystal-field levels
f^1 and f^{13}	^{2}F				2	14
f^2 and f^{12}	^{1}SDGI	^{3}PFH			13	91
f^3 and f^{11}	^{2}PDFGHIKL 2 2 2 2	^{4}SDFGI			41	364/2
f^4 and f^{10}	^{1}SDFGHIKLN 24 4 2 3 2	^{3}PDFGHIKLM 3 2 4 3 4 2 2	^{5}SDFGI		107	1001
f^5 and f^9	^{2}PDFGHIKLMNO 4 5 7 6 7 5 5 3 2	^{4}SPDFGHIKLM 2 3 4 4 3 3 2	^{6}PFH		193	2002/2
f^6 and f^8	^{1}SPDFGHIKLMNQ 4 6 4 8 4 7 3 4 2 2	^{3}PDFGHIKLMNO 6 9 7 9 6 6 3 3	^{5}SPDFGHIKL 3 2 3 2 2	^{7}F	295	3003
f^7	^{2}SPDF G HIKLMNOQ 2 5 7 10 10 9 9 7 5 4 2	^{4}SPDFGHIKLMN 2 2 6 5 7 5 5 3	^{6}PDFGHI	^{8}S	327	3432/2

For non-transparent compounds, neutron spectroscopy, paramagnetic resonance, specific heat and magnetic susceptibility are useful methods to investigate the splitting of the ground state multiplet, but they are very sensitive when a few crystal-field levels are involved.

In the following section we shall stress the influence of the crystal field which modifies the energy levels and wavefunctions of the free ion. However, as the free-ion levels are often unknown, the way of getting such information comes from theoretical considerations developed in the energy level calculations. Comparison of the energy levels obtained from the optical spectra with those calculated is the usual procedure to test the validity of the model under consideration.

Energy Level Calculations

The energy level structure within the f^n configuration in condensed media may be understood in terms of the free-ion levels with an additional interaction due to the crystal field. Then the centres of gravity of all crystal-field level sets may be related to the free-ion degenerate J levels, which are in turn related to the degenerate levels of the gaseous ion.

Free Ions

As a starting point, in the central-field approximation, each electron is assumed to move independently in an undefined spherically symmetric potential which originates from the nucleus and other electron electrical charges. To overcome the difficulty arising from the unknown potential in the energy level calculation, one can use the parametric approach [13] based on the separation of the variables which characterize the acting potential. Following this procedure, the angular part of the interaction is totally evaluated from geometrical considerations, while the radial integrals depending on the unknown potential are treated as parameters.

When the electrostatic and magnetic interactions between electrons are introduced, the Hamiltonian which describes the different interactions and then determines the f electron energy levels may be written as:

$$\mathcal{H} = H_0 + H_{ER} + H_{SO} + H_{CORR}$$

where the first term H_0 represents the kinetic energy of the f electrons and their coulomb interaction with the nucleus through an effective nucleus charge Z^*

$$H_0 = -\frac{h^2}{2m}\sum_{i=1}^{n}\nabla_i^2 - \sum_{i=1}^{n}\frac{Z^*e^2}{r_i}$$

As H_0 contains only spin-independent spherically symmetric terms, it does not remove any degeneracy within the f^n configuration and therefore is not taken into consideration.

For systems of two or more f electrons, the mutual electron–electron electrostatic repulsion, H_{ER}, splits the configuration into terms characterized by ^{2S+1}L according to the spin multiplicity and the total angular momentum L (Table II). The simplest form of this effective Hamiltonian into the framework of the parametric approach which considers the undefined radial part as a parameter, may be written as:

$$H_{ER} = \sum_k F^k f_k \qquad \text{(with } k = 0, 2, 4, 6 \text{ for f electrons; } k \leqslant 2l \text{ and is even)}$$

where f_k is the angular part of the interaction which can be evaluated from the symmetry of the system and F^k the Slater radial integral parameters determined empirically via a fitting procedure of the experimental data.

The spin–orbit interaction (between two magnetic dipoles), H_{SO}, removes the degeneracy of the ^{2S+1}L terms into J levels of the free-ion characterized by L, S, J quantum numbers ($^{2S+1}L_J$). This Hamiltonian can be written:

$$H_{SO} = \sum_i \zeta(r_i) l_i s_i$$

with for a hydrogen-like system:

$$\zeta(r) = \frac{h^2}{2m^2c^2} \frac{1}{r} \frac{\delta U(r)}{\delta r}$$

where $U(r)$ is the undefined potential in which the electron moves. In the parametric approach the Hamiltonian describing the spin–orbit interaction may be expressed as:

$$H_{SO} = \zeta_f A_{SO}$$

where A_{SO} is the angular part of the spin–orbit interaction and ζ_f the spin–orbit coupling constant adjusted to the experimental observed energies.

The model developed above gives the right order of magnitude of the parameters but it is not able to reproduce accurately all the experimental data. Some discrepancies remain between calculated and observed values and therefore it is apparent that the F^k and ζ associated purely with f^n configuration, cannot absorb all the effects. A better fit requires the introduction of new terms in the effective Hamiltonian. They are regrouped in H_{CORR} which represents higher order correction terms.

Rajnak and Wybourne [14] have shown that among the higher order electrostatically correlated perturbations, the dominant effects are the configuration interactions which occur between configurations of the same parity. It is a scalar two-body interaction which can be taken into account by additional two-electron operators through the following Hamiltonian:

$$H_1 = \alpha L(L+1) + \beta G(G_2) + \gamma G(R_7)$$

where α, β and γ are the parameters associated with the two-body interaction and $G(G_2)$, $G(R_7)$ are the Casimir operators for the groups G_2 and R_7.

By extension a three-body interaction (for system with $n \geqslant 3$) was formulated by Judd [15] and Crosswhite *et al.* [16], via the T^k parameters associated with three-particle operators:

$$H_2 = \sum_k T^k t_k \qquad \text{(with } k = 2, 3, 4, 6, 7, 8)$$

In addition to these coulomb interactions, Judd *et al.* [17] introduced higher-order magnetic effects due to configuration interactions and based on the fact that the admixture of an f′ state into a particular f state is spin dependent. The corresponding parameters are included in the following Hamiltonian:

$$H_3 = \sum_k P^k_{p_k} \qquad \text{(with } k = 2, 4, 6)$$

Further corrections of relativistic origin are namely the spin–spin interaction and the interaction between the spin of one electron and the orbital motion of another, called the spin–other orbit interaction. They are both represented by the Marvin integrals M^k

$$H_4 = \sum_k M^k m_k \qquad \text{(with } k = 0, 2, 4)$$

In the last three Hamiltonians, H_2, H_3, H_4, the lower-case letters account for the angular part of the interactions.

Since the 5f electrons in the actinides are more engaged in relativistic effects than 4f electrons in lanthanides, those parameters are expected to be larger for 5f than 4f ions.

Crystal-field Hamiltonian

The crystal-field interaction removes to a certain degree the degeneracy of the free-ion levels. The magnitude of the splitting of a J multiplet has been first parametrized in the simplest way assuming a static electrostatic field generated by the ion surrounding. In the crude charge point model (CPM) the ligand charges are assumed to be concentrated at the crystallographic position of the ions. A more realistic approach considers the charge density $\rho(R)$ of the environment to calculate the potential energy of an f electron:

$$V(r) = -\int \frac{e\rho(R)\,\mathrm{d}r}{(R - r)}$$

when R is the distance to a particular point of the environment and r is the distance of the electron.

According to the parametric approach, it is convenient to write the potential $V(r)$ in terms of B^k_q parameters with the Wybourne [18] formalism. The sum over the i electrons may be written as:

$$V_{CF} = \sum_{k,q,i} B^k_q C^k_q(\theta_i, \varphi_i)$$

where B^k_q are the crystal-field parameters (radial integrals)

TABLE III. Crystal Quantum Numbers for Different Higher Rank Crystal Axes

C_n	J integer		J half-integer Kramers doublet		
	Singlet	Doublet			
Twofold axis	$\mu = \pm 0, \pm 1$		1/2		
Threefold axis	± 0	1	1/2	3/2	
Fourfold axis	$\pm 0, \pm 2$	1	1/2	3/2	
Sixfold axis	$\pm 0, \pm 3$	1, 2	1/2	3/2	5/2

$$B_q^k = -e\int(-1)^q\rho(R)C_{-q}^k(\theta,\varphi)\frac{r^{k<}}{r^{>k+1}}\,d\tau$$

and C_q^k are tensor operators of rank k for the angular part of the crystal-field interaction.

The k and q values are determined in consideration of the symmetry of the site occupied by the f ion and are limited by the requirement that the crystal-field potential is invariant under the symmetry operations of the group. The crystal-field interactions mix states with different J values, so J and M_J are no longer good quantum numbers.

It is also possible to define equivalence classes of non-interacting sets of states characterized by different crystal quantum numbers μ defined as:

$$\mu = M_J \text{ (modulo } n)$$

where n is the order of the higher rank symmetry operator C_n or S_n (see Table III).

It must be remembered that the electrostatic model is based upon the following assumptions which make it mathematically practicable: the crystal field is a one-electron interaction which means that the f electrons are independent of each other and the crystal-field operator is defined within the limited space of free-ion spin-orbitals of unpaired electrons only.

This brief review of the parametric energy level calculations of an f^n ion in the solid state is summarized in Table IV which reports the different adjustable parameters to be evaluated from experimental data by a least-squares fitting procedure. If the amount of experimental data is not sufficient to

TABLE IV. Composition of the Parametric Hamiltonian[a]

	Interactions	Hamiltonians	Parameters	Labels	Quantum numbers
Dominant interactions free-ion Hamiltonian	core potential	$H_0 = p^2/2m$		configuration	n, l
	electronic repulsion ($n \geq 2$)	$H_{ER} = \sum_{k=0}^{6} f_k F^k$ (k even)	F^0, F^2 F^4, F^6	terms	L, S
	spin–orbit	$H_{SO} = A_{SO}\zeta_f$	ζ	J levels (free-ion)	L, S, J
Higher-order corrections free-ion Hamiltonian	two-body configuration interaction	$H_1 = \alpha L(L+1) + \beta G(G_2) + \gamma G(R_7)$	α, β, γ		
	three-body configuration interaction ($n \geq 3$)	$H_2 = \sum_k t_k T^k$	T^k (k = 2, 3, 4, 6, 7, 8)		
	magnetic effect due to configuration interaction	$H_3 = \sum_k p_k P^k$	P^k (k = 2, 4, 6)		
	spin–spin and spin–other orbit	$H_4 = \sum_k m_k M^k$	M^k (k = 0, 2, 4)		
Ion in solid state	crystal field interaction	$V_{CF} = \sum_{k,q,i} B_q^k (C_q^k)_i$	B_q^k k, q depend on site symmetry	crystal-field levels	μ

[a]From ref. 100.

support analyses in which all the listed parameters are varying freely, the higher order correction parameters can be held fixed (for M^k, identical to those computed using HF methods for example) or some parameter values can be constrained by fixing ratios to be held constant. The parametrization scheme of the total Hamiltonian reported here is able to reproduce satisfactorily the energy level structure of Ln^{3+} ions [19, 20], but interpretative problems remain for the 5f electron systems, especially for An^{4+} for which the standard deviations are appreciably larger. This acceptable agreement nevertheless says nothing about the validity of the model. As has been already pointed out, the different parameters absorb a variety of combined effects and the B_q^k values, for instance, describe the crystal field interaction only in a global way. The leading contributions such as electrostatic, covalency and overlap effects are difficult to evaluate separately. *A priori* calculations of crystal-field parameters are often carried out now using the superposition model developed by Newman [21]. This model is based on the assumption that the total crystal-field potential is a sum of separate contributions from each of the ions in the crystal. Introduction of the overlap [22] between f and ligand orbitals as a consequence of the non-orthogonality of the free-ion wavefunctions and the covalency effect [22, 24] due to charge transfer processes has provided a better basis for the *ab initio* calculations. In addition to these contact interactions, contributions from closed shells, referred to as shielding effects [25] and the ligand polarizability [26] are also considered, as well as the ligand–ligand electron exchange potential.

The superposition model calculations including all of these contributions provide crystal-field parameter sets which can be used to test the consistency of the experimentally evaluated parameters.

For further details about the theoretical considerations outlined in this section, one can refer to a number of books: Dieke [1], Ballhausen [27], Wybourne [18], Hüfner [28], Judd [29], Nielson and Koster [30] and Jorgensen [31].

Tetravalent Actinide Optical Spectroscopy

Among the tetravalent actinide ions, U^{4+} is the most widely studied ion for several reasons. First, the low-level radioactivity of uranium natural isotopes makes the doped single crystals easy to handle without any special precautions which is absolutely not the case for all the other actinides except thorium. In addition to this there is no limitation on the sample size and no noticeable radiation effects. These factors, added to the fact that the U^{4+} oxidation state in compounds is stable or easy to stabilize in selected optically clear hosts, set U^{4+} ions well apart from the other actinide tetravalent ions. Moreover, the f^2 configuration of U^{4+} provides experimental features in sufficient details to be suitable for theoretical analysis and to constitute a useful basis for extending the interpretation of spectra in condensed media. Recent U^V gaseous free-ion analyses [32, 33], rather sparse for An^{4+} ions, increase the knowledge of U^{4+} energy level structure and provide instructive correlations between free-ion and crystal spectra.

The situation has so far been less successful for the other An^{4+} ions. This results in a lack of suitable matrices into which the 4+ oxidation state can be stabilized. The promising $ThCl_4$ and $ThBr_4$ single-crystal hosts (which have to be compared to $LaCl_3$ and $LaBr_3$ for Ln^{3+} studies) brought interesting results for Pa^{4+} ($5f^1$) and U^{4+} ($5f^2$) but have failed for Np^{4+} ($5f^3$) where both 4+ and 3+ oxidation states were present, compromising the reliability of the level assignment. $ThSiO_4$ and $ZrSiO_4$ hosts (with some restriction due to the smaller Zr^{4+} radius) seem more appropriate for an investigation of the whole series, but a limitation arises from the flux crystal-growing technique which requires appreciable quantities of radioactive and expensive isotopic materials. As for Cs_2ThX_6 (X = Cl, Br) matrices, the presence of an inversion centre in the octahedral lattice symmetry makes the analysis of the almost pure vibronic spectra difficult, without the usual aid of the polarization effect. The actinide borohydrides $X(BH_4)_4$ and borodeuterides $X(BD_4)_4$ with $X = Pa^{4+}$, U^{4+}, Np^{4+} etc., diluted in $Hf(BH_4)_4$ have also been successfully prepared but their optical spectra show rich vibronic structure which may mask pure electronic spectral features. An attempt has also been made with $PbMoO_4$ host doped with Np^{4+}, but as Np^{4+} substitutes into a Pb^{2+} site, charge compensation is required and site distortion may occur. For the pure coloured An^{4+} compounds, part of the difficulty lies in the strong absorption of the photons, which can be overcome by adjusting the thickness of the sample prepared for transmission spectroscopy. Organometallic compounds [$(Et_4N)_4An(NCS)_8$, Cp_3AnCl (Cp = C_5H_5) etc.] fall into this category.

Most of the optical results presented herein were obtained in β-$ThBr_4$, β-$ThCl_4$ and $ThSiO_4$ host lattices. At room temperature the three crystals have a D_{4h}^{19} tetragonal structure ($I4_1/amd$) isostructural with UCl_4. In this structure the Th^{4+} ion is at a site of D_{2d} symmetry and according to the higher value of the Th^{4+} radius, the other An^{4+} ion can substitute into this site without any site distortion. A displacing phase transition was observed in β-$ThBr_4$ and β-$ThCl_4$ respectively at 95 K and 70 K [34] by Raman spectroscopy. Neutron diffraction experiments [35] revealed that the low temperature structure is incommensurate along the C_4 axis with a modulation of the halide-ion distances in a plane perpendicular to this axis. The sinusoidal distortion reduces the actinide

ion site symmetry from D_{2d} to D_2 with a continuous distribution of the different classes of site between the two limiting symmetries [36]. Laser selective site excitation experiments were able to sort out the respective absorption bands in D_{2d} and D_2 symmetries [37, 38].

Beyond these matrix considerations, it should be pointed out before going into further details that for An^{4+}, just as in An^{3+}, the crystal-field interaction cannot be considered as only a perturbation and therefore the total Hamiltonian must be diagonalized simultaneously. The J-mixing of the wavefunctions is then properly accounted for. Furthermore, owing to the strong spin–orbit coupling, wavefunctions are no longer pure Russel–Saunders wavefunctions but a linear combination of them. However we will keep the Russell–Saunders designation to give the largest contribution to the total wavefunction even if sometimes the mixing is so strong that the label is meaningless. Though intensity analysis will not be considered here, it is interesting to note that the absolute oscillator strengths of 5f transitions of U^{4+} in $ThBr_4$ and hydrobromic acid solution were found to be two orders of magnitude larger than those of 4f transitions and ten times larger than for U^{3+} [39]. The absorption spectra of An^{4+} in solution (Fig. 1) were of great help in interpreting the spectra in condensed media, especially in the weak field cases.

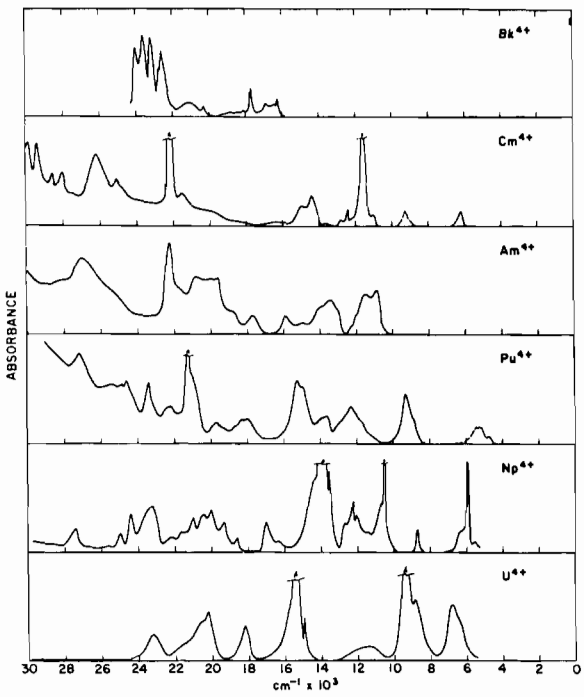

Fig. 1. Absorption spectra of tetravalent actinides in solution or solid state (from ref. 11 and refs. therein).

Protactinium Ion: Pa^{4+} ($5f^1$)

Only a few works have dealt with the optical spectroscopy of Pa^{4+}, the radioactivity of which represents a severe constraint. Data concerning optical and magnetic properties of Pa^{4+} doped into Cs_2ZrCl_6 were first reported by Axe [40] in an octahedral crystal-field symmetry. In the protactinium compounds $(Net)_2PaBr_6$ and $(Net)_2PaCl_6$, Edelstein *et al.* [41] have fitted optical data in a similar octahedral field and Amberger *et al.* [42] have reported data for $PaCl_4$ in D_{2d} symmetry. But all these works were based on an insufficient amount of experimental data and least-squares fitting can be justified only when the number of energy levels to be fitted exceeds the number of parameters; otherwise the parameters will be overdetermined.

In the case of Pa^{4+}:β-$ThBr_4$ and Pa^{4+}:β-$ThCl_4$ [43, 44], strong fluorescence was used to determine the energy of the low-lying Stark levels of the ground state $^2F_{5/2}$. Consequently all the seven doubly degenerate Kramer crystal-field levels into which the $5f^1$ configuration of Pa^{4+} splits under the influence of the spin-orbit and crystal-field interactions, were experimentally measured in the infrared region (Fig. 2). The assigned spectra characterized by two irreducible representations Γ_6 and Γ_7 of double group associated with D_{2d} symmetry, were fit by a least-squares routine to the parameters of the following Hamiltonian:

$$\mathcal{H} = \zeta ls + B_0^2C_0^2 + B_0^4C_0^4 + B_0^6C_0^6 + B_4^4(C_4^4 + C_{-4}^4) + B_4^6(C_4^6 + C_{-4}^6)$$

The best fit is reported in Table V. Table VI shows the six corresponding parameter values.

In the visible and near UV region, the intense emission spectra of Pa^{4+}:β-$ThBr_4$ and Pa^{4+}:β-$ThCl_4$ when irradiated with the 337.1 nm nitrogen laser line were assigned to 6d → 5f parity-allowed transitions in

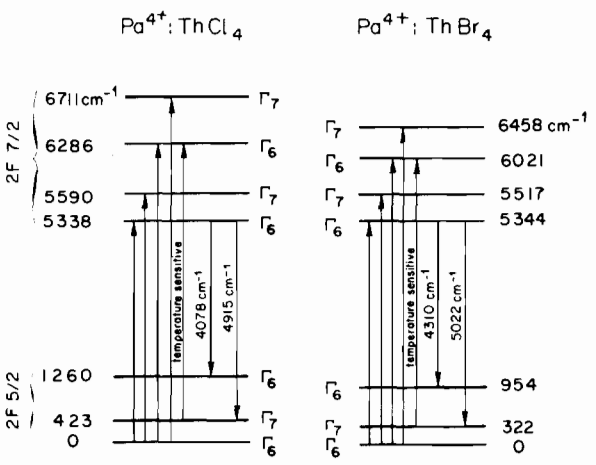

Fig. 2. Energy level diagram for Pa^{4+}:$ThBr_4$ and Pa^{4+}:$ThCl_4$.

TABLE V. List of Experimental and Calculated Energies for Pa^{4+} in $ThCl_4$ and $ThBr_4$

$L-S$ state	Pa^{4+}:$ThCl_4$		Pa^{4+}:$ThBr_4$		Irreducible representation
	Obs. (cm^{-1})	Calc. (cm^{-1})	Obs. (cm^{-1})	Calc. (cm^{-1})	
$^2F_{5/2}$	0	21.8	0	19.9	Γ_6
	423	408.8	322	313.9	Γ_7
	1260	1252.7	954	940.5	Γ_6
$^2F_{7/2}$	5338	5312.4	5344	5324.3	Γ_6
	5590	5605.8	5517	5522.6	Γ_7
	6286	6291.3	6021	6026.0	Γ_6
	6711	6715.1	6458	6464.8	Γ_7

TABLE VI. Spectroscopic Parameters of Pa^{4+} in $ThCl_4$ and $ThBr_4$ in D_{2d} Symmetry

Spectroscopic parameters[a, b]	Pa^{4+}:$ThCl_4$ [44] (cm^{-1})	Pa^{4+}:$ThBr_4$ [44] (cm^{-1})
ζ	1524.2 (5)	1532.8 (5)
B_0^2	−1404.8 (50)	−1046.5 (52)
B_0^4	1749.4 (94)	1366.3 (138)
B_4^4	−2440.3 (98)	−1990.1 (102)
B_0^6	−2404.2 (607)	−1162.0 (541)
B_4^6	−194.5 (267)	623.1 (174)

[a]Root mean squared = 23.6 cm^{-1} for Pa^{4+}:$ThCl_4$ and 19.4 cm^{-1} for Pa^{4+}:$ThBr_4$. [b]These sets of parameters are obtained for $F^0 = 3658$ cm^{-1} for Pa^{4+}:$ThCl_4$ and $F^0 = 3516$ cm^{-1} for Pa^{4+}:$ThBr_4$.

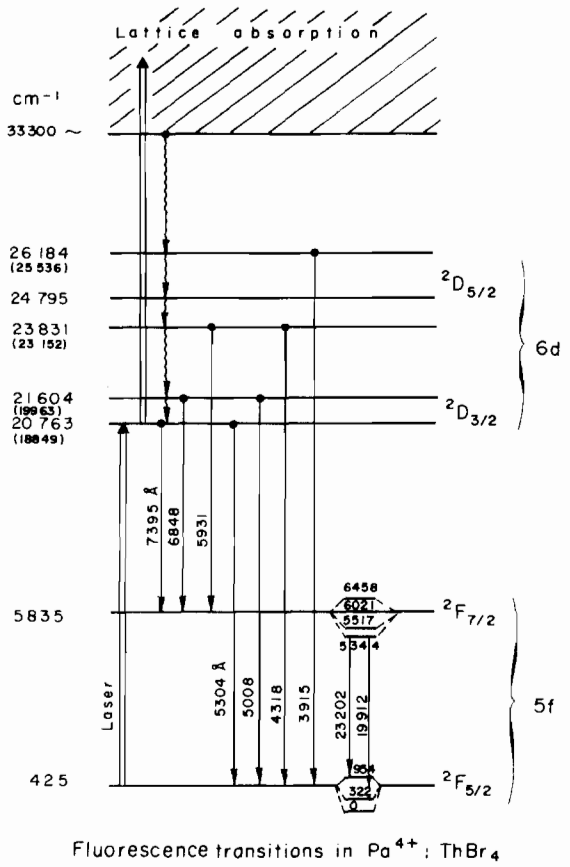

Fig. 3. f–d transitions in Pa^{4+}:$ThBr_4$.

Pa^{4+} [45]. A tentative energy level scheme (Fig. 3) was derived from the spectra but the entire energy spread of the 6d band appears to narrow and a missing level in the higher UV range should be found.

The radioluminescence (due to α and γ activities) which occurs in these crystals resembles in its intensity distribution among its spectral lines that observed in UV excitation, suggesting that the primary excitation in radioluminescence takes place in the lattice.

Uranium Ion: U^{4+} ($5f^2$)

New interest in the study of U^{4+} in the solid state started with the successful parametric analysis of U^{4+} in β-$ThBr_4$ [46] dealing with D_{2d} symmetry. On this basis, the new interpretation of the energy level structure of U^{4+} at a site of D_{2d} symmetry in the isomorphic $ThSiO_4$, β-$ThCl_4$ and UCl_4 has led to consistent sets of parameters when earlier published fits [47–57] were all quite tentative without any systematic trends.

Among the operations of the D_{2d} group of symmetry, there is no inversion centre and then zero-phonon transitions are expected. The $\sigma(E_\perp C_4$ and $\alpha(E, H_\perp C_4)$ spectra were checked to be the same, which according to the transformation properties of the electric-dipole operator, requires the use of electric-dipole selection rules. In all the investigated compounds with a D_{2d} site, a Γ_4 ground state for U^{4+} was assigned, which is consistent with the selection rules and MCD experiments which proved the ground state to be a non-degenerate level [58]. $\Gamma_4 \rightarrow \Gamma_1$ transitions are then observed on a π spectra ($E_\parallel C_4$) and $\Gamma_4 \rightarrow \Gamma_5$ transitions on σ spectra ($E_\perp C_4$).

Among the four systems, the U^{4+}:$ThSiO_4$ spectra [59] are the simplest with narrow lines and few vibronic components. The spectra get more complex with U^{4+}:$ThBr_4$ [46], U^{4+}:$ThCl_4$ [60] and UCl_4 [61]. In β-$ThBr_4$ and β-$ThCl_4$ the presence of an infinity of very close environments for the U^{4+} ions due to their incommensurate structures at low temperature, induces a broadening of the spectroscopic lines which can reach an appreciable width (up to 100 cm^{-1} for some $\Gamma_4 \rightarrow \Gamma_5$ transitions). In UCl_4, the broadening comes from the interactions between uranium ions and a marked vibronic structure. Despite the above mentioned differences the similarity of these spectra is a striking feature (Figs. 4, 5).

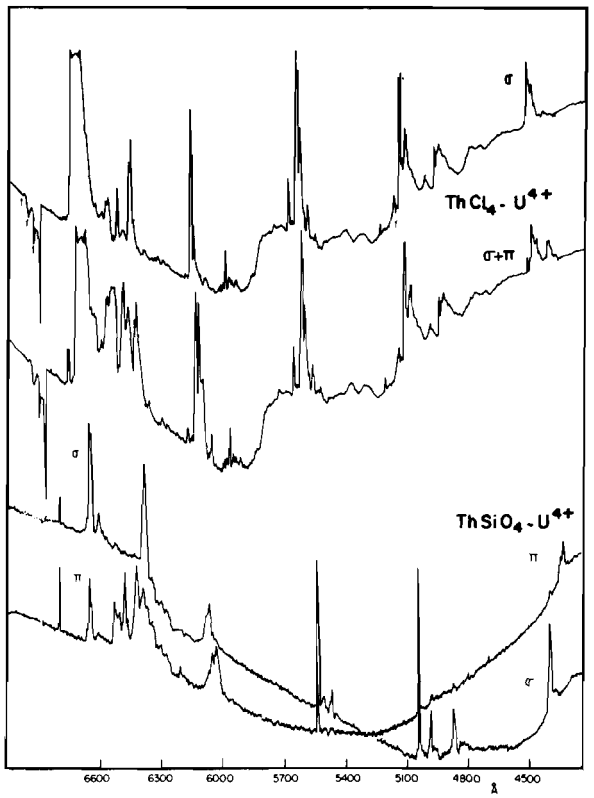

Fig. 4. Polarized spectra of U^{4+}:$ThCl_4$ and U^{4+}:$ThSiO_4$ in the visible region.

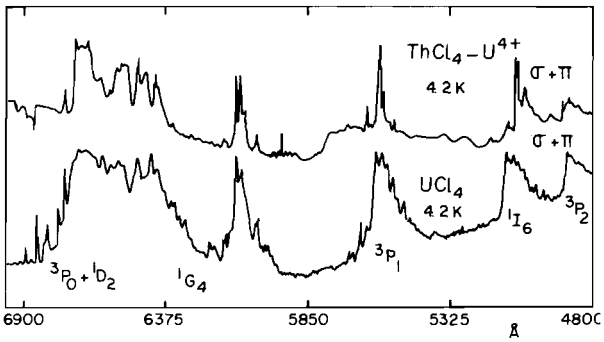

Fig. 5. Absorption spectra of U^{4+}:$ThCl_4$ and UCl_4 in the visible region.

The experimental levels were fitted by simultaneous diagonalization of the free-ion and crystal-field Hamiltonians characterized by the parameters of: interelectronic repulsion: F^k ($k = 2, 4, 6$); spin-orbit coupling: ζ; configuration interactions: α, β, γ; electrostatically correlated spin–orbit interactions: P^k ($k = 2, 4, 6$); spin–spin and spin–other orbit interactions: M^k ($k = 0, 2, 4$); crystal-field interactions: $B_0^2, B_0^4, B_4^4, B_0^6$ and B_4^6.

The better fit led to the parameters listed in Table VII. It should be noted that the energy levels are not very sensitive to the value of the B_4^6 parameter and it appears always poorly determined.

TABLE VII. Spectroscopic Parameters of U^{4+} in $ThSiO_4$, $ThCl_4$ and $ThBr_4$ in D_{2d} Symmetry

Spectroscopic parameters[a]	$ThSiO_4$:U^{4+} [59]	$ThCl_4$:U^{4+} [b] [60]	UCl_4 [b] [61]	$ThBr_4$:U^{4+} [b] [46]
F^2	43110 (245)	42752 (162)	42561 (235)	42253 (127)
F^4	40929 (199)	39925 (502)	39440 (634)	40458 (489)
F^6	23834 (639)	24519 (479)	24174 (185)	25881 (383)
F^4/F^2	0.95	0.93	0.93	0.96
F^6/F^2	0.55	0.57	0.57	0.61
ζ	1840 (2)	1808 (8)	1805 (8)	1783 (7)
α	32.3 (0.4)	30.4 (2)	30.9 (1)	31 (1)
β	−663 (144)	−492 (84)	−576 (168)	−644 (75)
γ	(1200)	(1200)	(1200)	(1200)
B_0^2	−1003 (127)	−1054 (117)	−903 (151)	−1096 (80)
B_0^4	1147 (281)	1146 (200)	766 (220)	1316 (146)
B_4^4	−2698 (251)	−2767 (147)	−3091 (185)	−2230 (85)
B_0^6	−2889 (557)	−2315 (404)	−1619 (482)	−3170 (379)
B_4^6	−208 (333)	−312 (227)	−308 (280)	686 (246)
$N_v(4\pi)^{-1/2}$ [c]	1342	1256	1224	1340
η [d]	25	25	26	26
σ [d]	71	46	60	36

[a] All parameters except γ vary. [b] $M^0 = 0.99; M^2 = 0.55; M^4 = 0.38; P^2 = P^4 = P^6 = 500$. [c] $N_v(4\pi)^{-1/2} = (\Sigma_k(\frac{1}{2}k + 1)(B_q^k)^2)^{1/2}$. [d] r.m.s. $\sigma = (\Sigma_{i=0}^{n}\Delta_i^2/n - m)^{1/2}$ where Δ_i is the difference between the calculated and observed energy level, n is the number of observed levels and m the number of varying parameters.

TABLE VIII. Spectroscopic Parameters of U^V free-ion and U^{4+} in $ThBr_4$ and $ThCl_4$ in D_{2d} and D_2 Symmetries[a]

Spectroscopic parameters	U^V [33] free-ion	D_{2d} symmetry		D_2 symmetry	
		$ThBr_4:U^{4+}$ [46]	$ThCl_4:U^{4+}$ [60]	$ThBr_4:U^{4+}$ [46]	$ThCl_4:U^{4+}$ [60]
F^2	51938 (39)	42253 (127)	42752 (162)	42264 (84)	42736 (175)
F^4	42708 (100)	40458 (489)	39925 (502)	41159 (407)	39821 (589)
F^6	27748 (68)	25891 (383)	24519 (479)	26018 (237)	24438 (470)
ζ	1968 (2)	1783 (7)	1808 (8)	1774 (5)	1805 (9)
α	33.5 (0.4)	31 (1)	30.4 (2)	[31]	31.6 (2.2)
β	−644 (25)	−644 (75)	−492 (84)	[644]	[−492]
γ	744 (26)	[1200]	[1200]	[1200]	[1200]
M^0		[0.99]	[0.99]	[0.99]	[0.99]
M^2		[0.55]	[0.55]	[0.55]	[0.55]
M^4		[0.38]	[0.38]	[0.38]	[0.38]
P^2	573 (66)	[500]	[500]	[500]	[500]
P^6	524 (144)	[500]	[500]	[500]	[500]
P^4	1173 (321)	[500]	[500]	[500]	[500]
B_0^2		−1096 (80)	−1054 (117)	−1108 (65)	−1037 (137)
B_0^4		1316 (146)	1146 (200)	1358 (137)	1121 (303)
B_4^4		−2230 (85)	−2767 (147)	−2219 (76)	−2948 (169)
B_0^6		−3170 (379)	−2135 (404)	−3458 (267)	−2120 (419)
B_4^6		686 (246)	−312 (227)	694 (195)	−315 (356)
B_2^2				−78 (30)	−77 (48)
B_2^4				318 (122)	356 (167)
B_2^6				136 (101)	158 (171)
B_6^6				123 (125)	424 (220)
n	13	26	25	38	34
σ	10	36	46	39	56

[a]All parameters in square brackets are held constant.

In D_2 symmetry, which is encountered also in U^{4+}:ThX_4 (X = Br, Cl) at low temperature, supplementary crystal-field parameters have to be added to account for the symmetry lowering: B_2^2, B_2^4 and B_6^6. The obtained parameter values are reported in Table VIII.

It should be emphasized that ThX_4 (X = Cl, Br) is one of the few matrices along with $ThSiO_4$ where U^{4+} is known to fluoresce in the solid state.

Special interest was shown in UCl_4 which has been studied in more detail [52, 53, 60]. In particular the $^3H_4$ ground manifold splitting was investigated by different methods (magnetic susceptibility [62] and neutron inelastic scattering [63, 64]) in order to establish the energy of the low-lying crystal-field levels. *A priori* calculations of the crystal-field parameters performed according to the superposition model have shown the importance of nonorthogonality and covalency effects [65]. The difference between the experimental and calculated value of the B_0^2 parameter suggested that the electrostatic polarization of the whole crystal-lattice cannot be ignored.

One has to mention the recent work on α-$ThBr_4$ host (space group $I4_1/a$) in which U^{4+} ions in S_4 local symmetry fluoresce strongly [66].

More extensive analysis of the spectra of U^{4+} have been published in higher symmetries, T_d and O_h, respectively in $U(BD_4)_4/Hf(BD_4)_4$ [67] and crystals containing UX_6^{2-} (X = Cl, Br) complexes such as Cs_2UCl_6 [68]. The largest crystal-field splitting and the consecutive higher B_q^k parameter values (Table IX) found for these two symmetries stand in contrast with the parameter values determined for U^{4+} in the D_{2d} symmetry of $ThBr_4$, $ThCl_4$, $ThSiO_4$ and UCl_4, which are characterized by a rather weak field interaction (Fig. 6).

To compare the magnitude of the different crystal-field strengths, it is convenient to use a scalar crystal-field parameter introduced by Auzel and Malta [69] and expressed as:

$$N_v/(4\pi)^{1/2} = \left[\sum_{k,q} (B_q^k)^2/2k + 1 \right]^{1/2}$$

TABLE IX. Spectroscopic Parameters of U^{4+} in O_h and T_d Symmetries[a]

Spectroscopic parameters	$U(BD_4)_4/Hf(BD_4)_4$ T_d site symmetry [67]	UCl_6^{2-} O_h site symmetry [68]	
F^2	41280 (175)	41175	42266 (760)
F^4	40013 (826)	40838	39604 (3331)
F^6	22554 (625)	28858	26360 (2017)
ζ	1782 (12)	1792	1760 (28)
α	38 (2)		[31]
β	[648]		[644]
γ	[1200]		[1200]
M^0	[0.99]		[0.99]
M^2	[0.55]		[0.55]
M^4	[0.38]		[0.38]
P^2	[500]		[500]
P^4	[500]		[500]
P^6	[500]		[500]
B_0^4	−2445 (124)	7656	7797 (394)
B_0^6	−5371 (81)	1472	1344 (230)
No. of levels	19	23	23
σ	52	>150	189
$N_v/4\pi$	4346		3562

[a]All parameters in square brackets held constant. For T_d or O_h symmetry, $B_4^4 = (5/4)^{1/2}B_0^4$, $B_4^6 = -(7/2)^{1/2}B_0^6$.

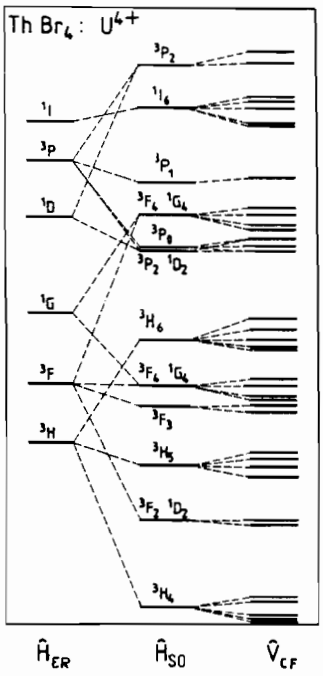

Fig. 6. Energy levels diagram for U^{4+}:$ThBr_4$ (from ref. 98).

N_v is a number which characterizes the crystal-field strength in any kind of site symmetry and then permits cross-comparison between different crystals.

In an octahedral crystalline field, since the dipolar electronic transitions are forbidden because of an inversion centre, the U^{4+} absorption spectra are essentially vibronic with several weak magnetic dipole transitions. As actinides couple much more than lanthanides with the lattice, actinides generally display rich vibronic spectra. The observed pure electric transitions are associated to a local distortion caused by lattice imperfections. The parametric analysis results in a r.m.s. deviation greater than 100 cm^{-1} (one order higher than those obtained in lanthanides). The parameters obtained by Satten *et al.* [68] for the hexachloro complex are listed in Table IX.

Uranium organometallic compounds have, up to now, never been really successfully assigned [70–72]. The general disagreement could be attributed to a lack of oriented crystals or to a use of approximate symmetries to characterize unequivalent sites which arise in salts containing large cation complexes.

Neptunium Ion: Np^{4+} ($5f^3$)

Formally, the Np^{4+} crystal energy level structure is equivalent to its lanthanide analogue Nd^{3+} ($4f^3$) but the interpretation of optical data has led to the conclusion that the comparison is not so straightforward. The larger spin–orbit coupling combined to larger crystal-field interactions on one hand mix strongly the *SLJ* character of the levels and, on the other hand, induce important overlappings of the excited crystal-field levels as the energy increases (Fig. 7). Because of this high density of states, only the Stark components of the four lowest manifolds, $^4I_{9/2}$, $^4I_{11/2}$, $^4F_{3/2}$ and $^4I_{13/2}$, which are well-isolated can be reasonably assigned and fitted for parametric analysis in condensed media. As the crystal-field splitting is smaller than the quadruplet separation, J can be considered as a good quantum number for these four manifolds. Fluorescence occurs generally from quadruplet $^4I_{11/2}$, therefore the ground state structure, which cannot be found through absorption, can be well determined as was shown for the Np^{4+}:$PbMoO_4$ [73] and Np^{4+}:$ThSiO_4$ [74] systems. Exceptionally, in the visible region, the relatively pure $^4G_{7/2}$ manifold situated on one side of an energy gap can be accurately assigned, thus increasing the small amount of reliable experimental data to be fitted.

In Np^{4+}:$ThSiO_4$, the D_{2d} crystal-field symmetry splits the free-ion J levels into Kramer doublets designated by Γ_6 and Γ_7 irreducible representations of the D_{2d} group. They are associated respectively with the crystalline quantum numbers $\mu = 1/2$ and $\mu = 3/2$. The diagonalization of the full Hamiltonian

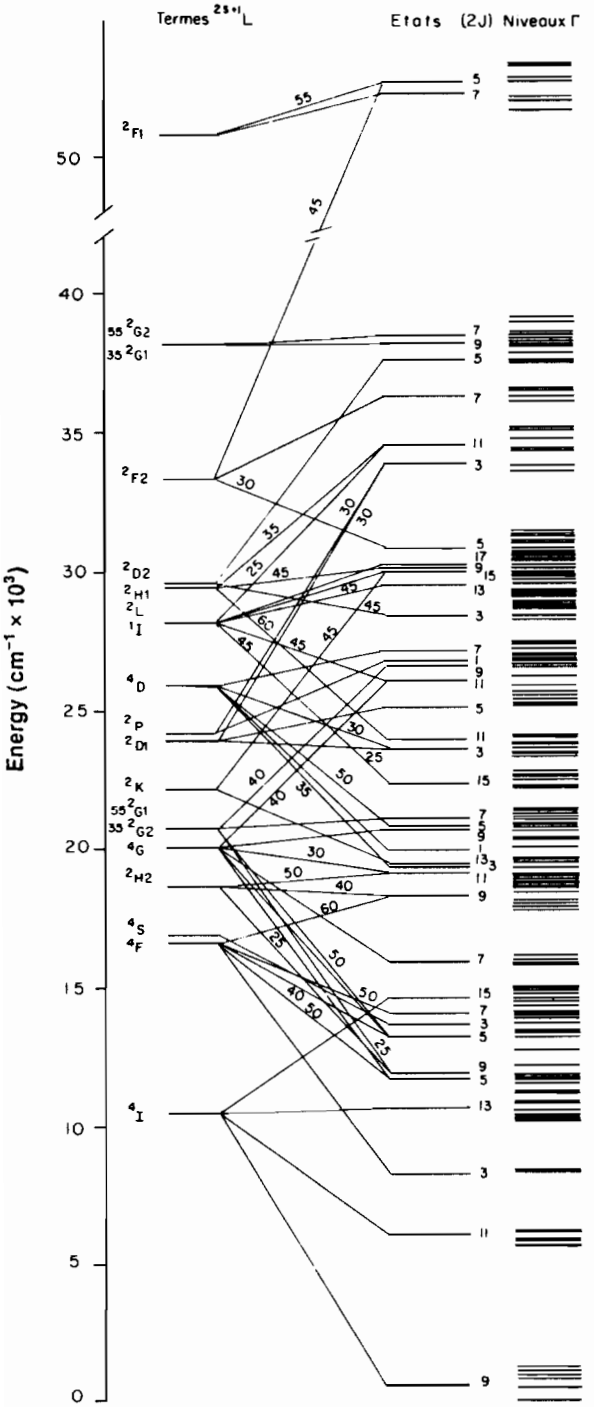

Fig. 7. Energy levels diagram for Np^{4+}:$ThSiO_4$ (from ref. 99).

including the three-body configuration interaction parameters T^k ($k = 2, 3, 4, 6, 7, 8$) followed by the usual least-squares fitting procedure has provided the parameters listed in Table X. Twenty-nine levels were assigned with a r.m.s. of 46 cm^{-1}. The comparison with the crystal-field parameters obtained for U^{4+}:$ThSiO_4$ shows some discrepancies, especially for B_0^2, but the positive sign accounts for the polarization of the $^4F_{3/2}$ manifold.

In an earlier work, the energy level structure of Np^{4+} in $PbMoO_4$ [73] was investigated in an S_4 local symmetry which is a subgroup of D_{2d}. The absorption and emission regions are quite similar in both crystals but $ThSiO_4$ provided more detailed spectra. Calculations involving only the five lowest multiplets were based on a first-order crystal-field model with initial free-ion parameter values proposed by Conway [75] (interpreting Np^{4+} spectra in solution [76]) and without including J mixing. However, this attempt represents the first important contribution to Np^{4+} spectroscopy in the solid state.

An Np^{4+}:$ZrSiO_4$ study was also recently undertaken, in D_{2d} symmetry [77]. Though the main features are identical to those recorded on Np^{4+}:$ThSiO_4$, the fitted parameters (Table X) are surprisingly different. The large discrepancies in the B_q^k values reveal the difficulties encountered with Np^{4+} ion spectroscopy which will remain for a while, an open field for further investigation.

An example of higher symmetry cases was provided by the extensively studied $Np(BD_4)_4/Zr(BD_4)_4$ system [78]. In the Td symmetry, the Np^{4+} ion levels are designated by Γ_6, Γ_7 and Γ_8 irreducible representations with respective degeneracies 2, 2 and 4. As has been already pointed out for U^{4+} ions doped in the same host, the large number of vibronic transitions give rise to many ambiguities in the identification of pure electronic transitions. Nevertheless, a very coherent determination of the parameter values was carried out by adopting comparative approaches. The first-order free-ion parameter ranges were determined by assuming that the same differences exist between U^{3+} and Np^{3+} in $LaCl_3$ on one side and U^{4+} and Np^{4+} in $U(BD_4)_4$ and $Np(BD_4)_4$ on the other side. Constant differences were also assumed between the pseudo-relativistic Hartree–Fock calculated values and the parameter values determined from $U(BD_4)_4$ and $Np(BD_4)_4$. A total of 46 zero-phonon transitions were assigned and fitted with a r.m.s. of 84 cm^{-1}. The obtained parameters are listed in Table X.

In octahedral and cubic crystal fields, data have been published for Cs_2NpCl_6 [79], $[(C_2H_5)_4N]_2$-$NpCl_6$ [80] and ThO_2 [81] where Np^{4+} ions occupy a site of inversion symmetry. The recent Np^{4+}:ThO_2 analysis [74] has shown the vibronic character of the spectra in contradiction with the previous work [81], where small distortions removing the inversion centre were supposed in order to allow weak forced electric dipole transitions. Only 16 accurate levels were considered, which is not far enough, with regards to the parameter number, to describe fully the energy levels of Np^{4+}. Thus, only a tentative fit which is certainly not unique, was proposed (Table X).

TABLE X. Spectroscopic Parameters of Np^{4+} in Different Matrices[a]

Spectroscopic parameters	Np^{4+}:$ThSiO_4$ D_{2d} [74]	Np^{4+}:$ZrSiO_4$ D_{2d} [77]	$Np(BD_4)/Zr(BD_4)_4$ T_d [78]	Np^{4+}:ThO_2 O_h (cubic) [74]
F^2	45196 (716)	46259	46689 (415)	49269 (968)
F^4	38032 (546)	44193	43239 (645)	37662 (1080)
F^6	28343 (791)	25463	26303 (722)	30937 (1434)
ζ	2129 (7)	2076	2089 (10)	2175 (13)
α	15 (3)		40 (2)	18 (3)
β	[−600]		[−600]	[−600]
γ	[1200]		[1200]	[1200]
B_0^2	323 (185)	−2104		
B_0^4	1511 (278)	4434	−2722 (182)	−854 (281)
B_4^4	−3559 (163)	−5251		
B_0^6	−1871 (372)	−4879	−5070 (69)	−994 (142)
B_4^6	−801 (197)	−79		
No. of levels	29	37	46	16
σ	47	75	84	74

[a]In T_d or O_h symmetry $B_4^4 = (5/14)^{1/2}B_0^4$, $B_4^6 = -(7/2)^{1/2}B_0^6$. For all calculations, the values of the parameters $M^0 = 0.88$, $M^2 = 0.49$, $M^4 = 0.34$, $P^2 = P^4 = P^6 = 500$, $T^2 = 278$, $T^3 = 44$, $T^4 = 64$, $T^6 = -361$, $T^7 = 434$, and $T^8 = 353$ cm^{-1} were used. Values in square brackets were held constant. All parameters are in cm^{-1}.

Plutonium Ion Pu^{4+} ($5f^4$) and Heavier An^{4+} Ions

While for tetravalent actinide, spectra of the aqua ions or in the solid state (usually XF_4) have been obtained for many years up to Cf^{4+} (Fig. 1), reliable parameter values for the heavier An^{4+} ions are rather sparse, even for Pu^{4+}.

Recently, Pu^{4+}:$ThSiO_4$ and Am^{4+}:$ThSiO_4$ crystals were grown with the flux technique and polarized absorption spectra were recorded for the Pu^{4+} ion (Fig. 8). Preliminary calculations, using parameters deduced from Np^{4+}:$ThSiO_4$, reproduce fairly well the main features as far as the absorption regions and the energy gaps.

Furthermore, anhydrous solid americium tetrafluoride, $^{241}AmF_4$, has been prepared [82] as well as CmF_4 [83], BkF_4 [84] and CfF_4. Absorption spectra of these fluorides have been recorded and fluorescence was recently observed for $^{249}Bk^{4+}$ in CeF_4 [85].

Attempts to interpret some of these spectra have been published [86, 87] but the results should be considered preliminary and, certainly, many works remain unpublished because of a lack of valuable basis. For these reasons, the predictive model proposed by Crosswhite, Crosswhite and Carnall [11, 13, 88, 89] is of great importance.

The C.C.C. Predictive Model

The systematic interpretation of the trivalent lanthanide and actinide spectra has shown that the

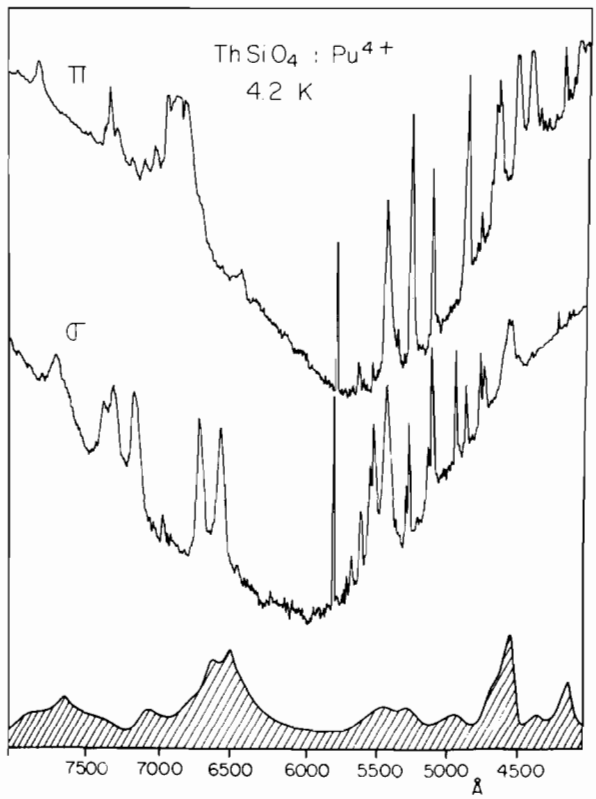

Fig. 8. Pu^{4+}:$ThSiO_4$ polarized absorption spectra in the visible range – the absorption of Pu^{4+} in $DClO_4$ is reported in grey for comparison.

TABLE XI. Energy Level Parameters for An^{3+} Based on the Predictive Model[a]

	U^{3+}	Np^{3+}	Pu^{3+}	Am^{3+}	Cm^{3+}	Bk^{3+}	Cf^{3+}	Es^{3+}
F^2(HFR) [b]	71442	74944	78223	81346	84331	87192	89964	92657
F^2(FIT) [c]	39715	44907	48670	51800	55109	57015	61014	62766
Difference	31727	30037	29553	29546	29222	30177	28950	29891
F^4(HFR)	46370	48733	50942	53044	55049	56969	58826	60629
F^4(FIT)	33537	36918	39188	41440	43803	45698	44483	48003
Difference	12833	11815	11754	11604	11246	11271	14343	12626
F^6(HFR)	33918	35684	37335	38905	40403	41826	43222	44567
F^6(FIT)	23670	25766	27493	30050	32610	33552	36168	35309
Difference	10248	9918	9842	8855	7793	8274	7054	9258
ζ(HFR)	1898	2182	2479	2792	3119	3463	3824	4023
ζ(FIT)	1623	1938	2241	2580	2903	3216	3568	3962
Difference	275	244	238	212	216	247	256	241

[a]From ref. 11. [b]Computed using Hartree–Fock methods and including an approximate relativistic correction [6, 90]. [c]Computed by fitting to experimental data.

trend in the fitted values of F^k and ζ free-ion parameter, as a function of the atomic number Z, follows roughly the variation of the corresponding calculated Hartree–Fock values [90]. The variations are not linear, but the difference between the two sets of values, *versus* Z, appears nearly constant over the whole series (Table XI). Thus, if the analysis of one element of the series has provided reliable parameters, the extrapolation procedure proposed by the model can predict the energy level structure of the other members.

This model was applied to calculate the An^{4+} ion energy level diagrams (Fig. 9) using the ThX_4:U^{4+} parameter values as a basis for the weak crystal-field case (Table XII). Concerning this point, one can notice that the U^{4+}:$ThBr_4$ absorption spectrum is well correlated with the observed spectrum for the U^{4+} aqua ion (Fig. 10).

This new approach is very useful to test the accuracy of experimentally determined parameter values or to provide first sets of parameters to initiate calculations.

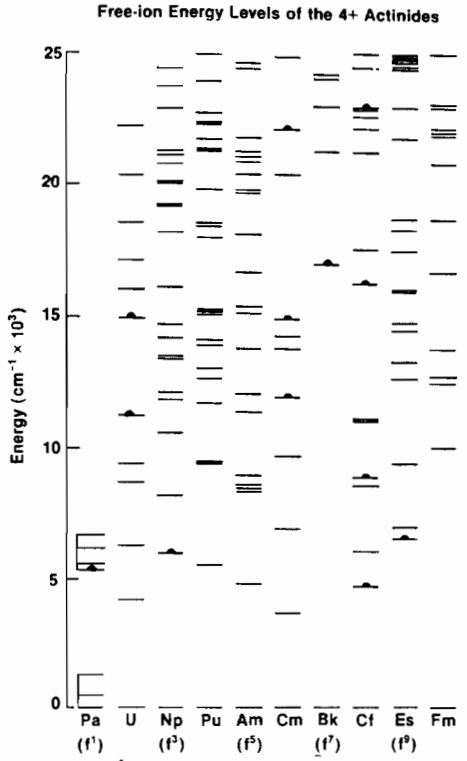

Fig. 9. An^{4+} energy level diagram based on the predictive model (from ref. 11).

Comparison Between Actinides and Lanthanides

When the parameters issued from the $5f^n$ ion parametric analyses are compared to those obtained for the $4f^n$ ions for configurations with the same number of f electrons (Table XIII), the striking features are: the reduction of the F^k Slater parameters (Fig. 11); the large increase in the spin–orbit coupling constant (Fig. 12); the larger crystal-field parameters (Fig. 13).

Because of the reduction in the electronic repulsion, the energy ranges for $5f^n$ configurations are reduced when the larger spin–orbit and crystal-field interactions shorten the energy gaps between J levels. Then, overlappings and density of levels increase considerably with excitation energy (Fig. 14) and consequently J level orderings for An^{4+} ions are different from those for the corresponding Ln^{3+} ions.

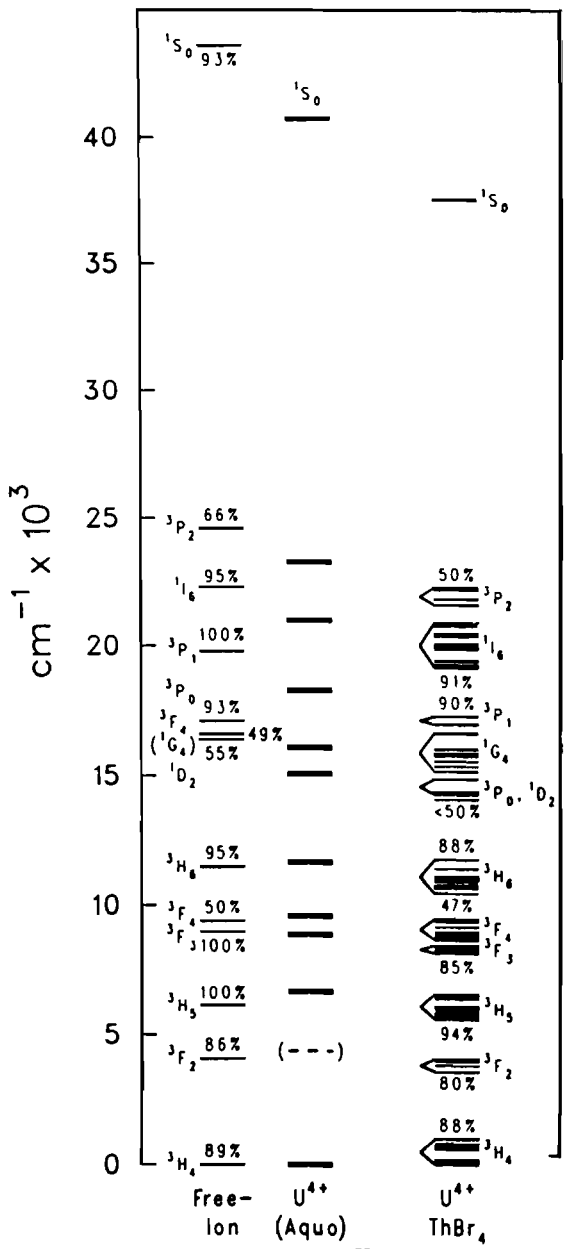

Fig. 10. Energy levels diagram for U^{V}, U^{4+} aqua and U^{4+} in $ThBr_4$ (from ref. 11).

Furthermore, the larger ζ values mix the S, L character of the An^{4+} levels more. In addition, the admixing of J states due to larger B_q^k values becomes greater and reduces the selection rule effects. Simultaneously, the odd crystal-field parameters induce comparatively larger admixing of opposite parity states into $5f^n$ configuration, increasing the intensity of the forced electric dipole transitions.

The dynamic crystal-field interactions and ion–phonon coupling will also be greater for the actinides, increasing the probability of vibronic transitions.

Comparison between the Hartree–Fock calculated values for Ln^{3+} and An^{4+} and those empirically determined from optical spectra in the solid state shows also some more trends. The difference in F^2 parameter values (Fig. 10) is due essentially to the combination of two effects: the configuration interaction and, to a less amount, the depression of high levels by the crystal environment [91]. But, as was already pointed out, the 5f orbitals are more extended than 4f ones and thus one can expect more configuration interaction and a greater sensitivity to the crystal field for An^{4+}. These two factors explain the larger reduction of F^2 for An^{4+} than for Ln^{3+}, while F^4 and F^6 which are less affected by the configuration interaction are less reduced. The particular crystal-field effect underlined above is expected to be magnified in the high symmetry cases, O_h and T_d, where the crystal-field strengths are approximately twice as large as those found for the lower symmetry D_{2d}. The F^k values determined for U^{4+} ions respectively in Cs_2UX_6 (X = Cl, Br), $U(BD_4)_4$ and ThX_4 (X = Cl, Br) show this evolutive trend: the F^k values increase as the crystal-field strength decreases (Tables VII, IX).

For the parameters F^k and ζ, the difference between their values for the free-ion and the ion in the solid state is often referred to as the nephelauxetic effect [92]. The ratio $\beta = F^2_{\text{crystal}}/F^2_{\text{free-ion}}$ can be used as a measure of the effect and provides an indication of the degree of covalency in the ion-bonding. Indeed, the nephelauxetic series, in terms of the magnitude of the effect for inorganic compounds, can be expressed as:

$$\text{Free-ion} < F^- < O^{2-} < Cl^- < Br^- < I^- \simeq S^{2-} < Se^{2-} < Te^{2-}$$

which is equivalent to the ionicity or covalency ordering (F^- being the least covalent ion).

This order is well reproduced for the β ratio found in U^{4+}:$ThSiO_4$, U^{4+}:$ThCl_4$ and U^{4+}:$ThBr_4$ which takes respectively the values 0.83, 0.82 and 0.81 (Table XIV). The F^2 reduction makes the 5f electrons of U^{4+} act more like 3d than 4f electrons. But according to Newman [93], the nephelauxetic series cannot be determined by the degree of admixture between ligand and f open-shell wavefunctions and is related only to the ligand polarizability. His demonstration is based upon the fact that the spectrochemical series where the ligands are ordered by the magnitude of the crystal-field splitting, due essentially to overlap and covalency, is opposite to the nephelauxetic ordering. The B_q^k values obtained for Pa^{4+}:$ThCl_4$ and Pa^{4+}:$ThBr_4$ [Table VI] follow fairly well the spectrochemical series which can be expressed as:

$$\text{Free ion} < I^- < Br^- < Cl^- < S^{2-} < F^- < O^{2-}$$

TABLE XII. Energy Level Parameters for An^{4+} Based on the Predictive Model[a]

	U^{4+}	Np^{4+}	Pu^{4+}	Am^{4+}	Cm^{4+}	Bk^{4+}	Cf^{4+}	Model value
F^2(HFR) [b]	76724	79892	82908	85817	88625	91338	93984	
F^2(Est) [c]	42918	46090	49110	52020	54825	57540	60185	
Difference	33806	33802	33798	33797	33800	33798	33799	33800
F^4(HFR)	50199	52330	54356	56307	58188	60003	61772	
F^4(Est)	39873	42000	44030	45980	47860	49670	51440	
Difference	10326	10330	10326	10327	10328	10333	10332	10330
F^6(HFR)	36860	38452	39965	41423	42827	44181	45500	
F^6(Est)	25588	27180	28695	30150	31555	32910	34230	
Difference	11272	11272	11270	11273	11272	11271	11270	11270
ζ(HFR)	2110	2397	2697	3014	3347	3697	4064	
ζ(Est)	1810	2095	2395	2715	3045	3395	3765	
Difference	300	302	302	299	302	302	299	300

[a]From ref. 11. In addition to the free-ion parameters shown, the following parameter values (in cm^{-1}) were used in all calculations: $\alpha = 30.12$; $\beta = -660$; $\gamma = 1200$; $B_0^2 = -1129$, $B_0^4 = 1793$, $B_4^4 = -2617$, $B_0^6 = 3016$, $B_6^6 = 342$; $p^2 = 500$, $p^4 = 375$, $p^6 = 250$. For $5f^n$ where $n \geqslant 3$, threebody parameters were included and the values assigned were: $T^2 = 200$, $T^3 = 50$, $T^4 = 100$, $T^6 = -300$, $T^7 = 400$, $T^8 = 350$. [b]Computed using Hartree-Fock methods and including an approximate relativistic correction [6, 90]. [c]Parameter value used to compute the energy level structure. The set for U^{4+} was estimated for U^{4+}:$ThCl_4$ [60].

TABLE XIII. Comparison Between the Pr^{3+} ($4f^2$) and U^{4+} ($5f^2$) Spectroscopic Parameters in D_{2d} Symmetry

Spectroscopic parameters	$ThCl_4$:Pr^{3+} [94]		$ThBr_4$:Pr^{3+} [95]	$LuPO_4$:Pr^{3+} [96]	YPO_4:Pr^{3+} [96]	$ThBr_4$:U^{4+} [46]	$ThCl_4$:U^{4+} [60]
	Set 1	Set 2					
F^2	67947	67866	68354	67688	67779	42253	42752
F^4	50576	50219	50310	48633	49603	40458	39925
F^6	33468	33322	33799	32151	32413	25881	24519
ζ	742	742	739	744	739	1783	1808
α	21	19	21	21	21	31	30
$\beta/12$	−39	−43	−67	−55	−55	−54	−41
γ	1343	1343	1343	1534	1534	1200	1200
B_0^2	545	20	260	21	78	−1096	−1054
B_0^4	−657	292	−644	280	321	1316	1146
B_4^4	876	−964	929	−808	−849	−2230	−2767
B_0^6	1398	−1525	1089	−1658	−1377	−3170	−2135
B_4^6	508	52	241	291	35	686	−(312)
Number of levels	52	52	42	18	35	26	25
σ (cm^{-1})	34	66	61	27	15	36	46

TABLE XIV. Comparison of the β Ratio for Different Environments

Complex	$\beta = F^2$ (crystal)/F^2 (free ion)	B (crystal)/B (free ion)	References
$U(BD_4)_4$ in $UF(BD_4)_4$	0.79		67
Cs_2UX_6 (X = Br)	0.80		54
(X = Cl)	0.81		54
$ThSiO_4$:U^{4+}	0.83		59
ThX_4:U^{4+} (X = Br)	0.81		46
(X = Cl)	0.82		60
UCl_4	0.82		61
$LaCl_3$:Pr^{3+} ($4f^2$)	0.93		6
Cr^{3+} ($3d^3$) in K_2NaCrF_6		0.83	97

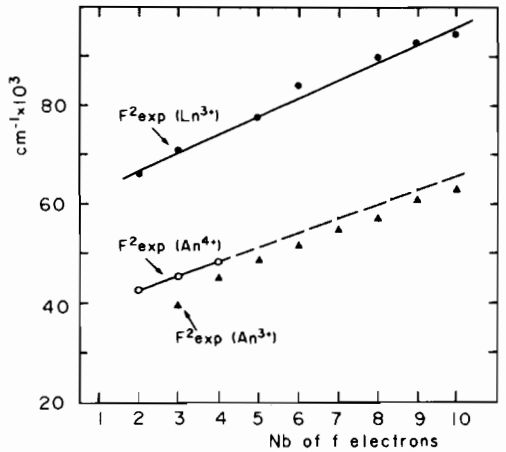

Fig. 11. Variation of the experimental values of the F^2, Slater parameter for Ln^{3+}, An^{3+} and An^{4+} *vs.* Z.

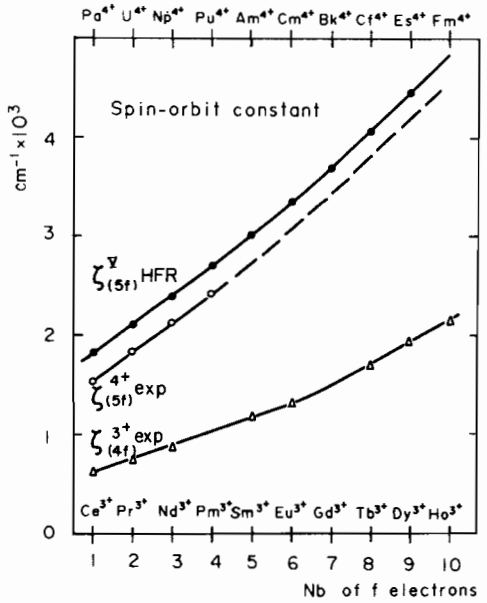

Fig. 12. Variation of the experimental spin–orbit constant values *vs.* Z, for the An^{4+} and Ln^{3+}. The pseudo-relativistic Hartree–Fock calculated values for An^{V} are reported for comparison.

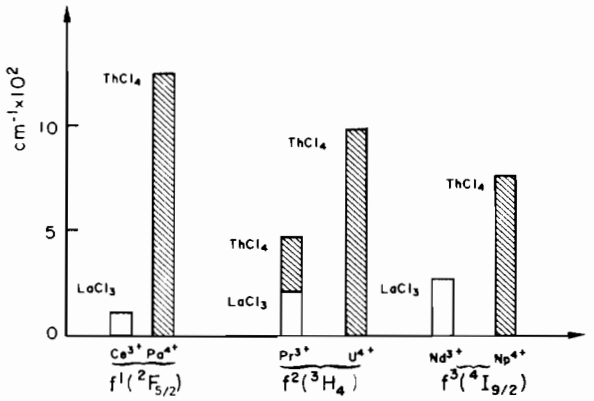

Fig. 13. Comparison of the crystal-field splitting of the ground-state manifold of lanthanide and actinide ions with the same f^n configuration.

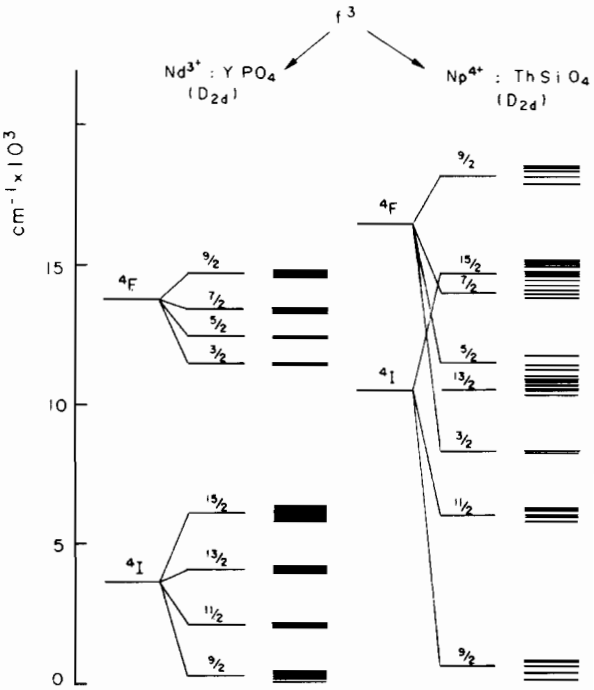

Fig. 14. Comparison of the splitting of the two lowest terms for the f^3 configuration of Nd^{3+} and Np^{4+} in D_{2d} symmetry.

Unfortunately, this is not the case for U^{4+} in $ThBr_4$, $ThCl_4$ and $ThSiO_4$ where no obvious trend appears.

For these reasons, as well as for the relatively important standard deviation found in reproducing the An^{4+} optical data, there is some evidence that the crystal-field model is not able to account for all the effects and some more refinements are expected. Special attention has to be drawn to the fact that the standard deviation increases when the crystal-field strength becomes larger.

References

1 G. H. Dieke, 'Spectra and Energy Levels of Rare Earth Ions in Crystals', Wiley, Interscience, New York, 1968, and refs. therein.

2 W. T. Carnall, H. Crosswhite and H. M. Crosswhite, 'Energy Level Structure and Transition Probabilities of the Trivalent Lanthanides in LaF_3', *Argonne National Laboratory Report*, 1977, and refs. therein.

3 G. F. Koster, J. O. Dimmock, R. C. Wheeler and H. Statz, 'Properties of the Thirty-two-Point Groups', M.I.T. Press, Cambridge, Mass., 1963.

4 C. A. Morrison and R. P. Leavitt, *J. Chem. Phys., 71,* 2366 (1979).
5 W. T. Carnall, G. L. Goodman, R. S. Rana, P. Vandevelde, L. Fluyt and C. Görller-Walrand, *J. Less-Common Met., 116,* 17 (1986).
6 H. M. Crosswhite, 'Spectroscopie des Eléments de Transition et des Eléments Lourds dans les Solides, Colloque Internat. CNRS, 28 June 1976', Edition du CNRS, Paris, 1977.
7 P. Porcher and P. Caro, *J. Chem. Phys., 68,* 4176 (1978).
8 H. Lammermann and J. G. Conway, *J. Chem. Phys., 38,* 259 (1963).
9 J. B. Gruber, W. R. Cochran, J. G. Conway and A. T. Nicol, *J. Chem. Phys., 45,* 1423 (1966).
10 W. T. Carnall, H. Crosswhite, H. M. Crosswhite, J. P. Hessler, N. Edelstein, J. G. Conway, G. V. Shalimoff and R. Sarup, *J. Chem. Phys., 72,* 5089 (1980).
11 W. T. Carnall and H. M. Crosswhite, 'Optical Spectra of Actinide Ions in Compounds and in Solution', *Argonne National Laboratory Report, ANL-84-90,* 1985.
12 M. Hussonois, J. C. Krupa, M. Genet, L. Brillard and R. Carlier, *J. Cryst. Growth, 51,* 11 (1981).
13 H. M. Crosswhite and H. Crosswhite, *J. Opt. Soc. Am., B1,* 246 (1984).
14 K. Rajnak and B. G. Wybourne, *Phys. Rev., 132,* 280 (1963).
15 B. R. Judd, *Phys. Rev., 141,* 4 (1966).
16 H. Crosswhite, H. M. Crosswhite and B. R. Judd, *Phys. Rev., 174,* 89 (1968).
17 B. R. Judd, H. M. Crosswhite and H. Crosswhite, *Phys. Rev., 169,* 130 (1968).
18 B. G. Wybourne, 'Spectroscopic Properties of Rare Earths', Interscience, New York, 1965.
19 J. P. Hessler and W. T. Carnall, 'ACS Symposium Series', No. 131, American Chemical Society, Washington D.C., 1980, p. 349.
20 F. S. Richardson, M. F. Reid, J. J. Dallara and R. D. Smith, *J. Chem. Phys., 83,* 3813 (1985).
21 D. J. Newman, *Adv. Phys., 20,* 197 (1971).
22 O. L. Malta, *Chem. Phys. Lett., 87,* 27 (1982).
23 B. R. Judd, *J. Phys. C, 13,* 2695 (1980).
24 M. M. Ellis and D. J. Newman, *J. Chem. Phys., 49,* 4037 (1968).
25 R. M. Sternheimer, M. Blume and R. F. Peierls, *Phys. Rev., 173,* 376 (1968).
26 M. T. Hutchings and D. K. Ray, *Proc. Phys. Soc. (London), 81,* 663 (1963).
27 C. J. Ballhausen, 'Introduction to Ligand Field Theory', (Series in Advanced Chemistry), McGraw-Hill, New York, 1962.
28 S. Hufner, 'Optical Spectra of Transparent Rare Earth Compounds', Academic Press, New York, 1978.
29 B. R. Judd, 'Operators' Techniques in Atomic Spectroscopy', McGraw-Hill, New York, 1963.
30 C. W. Nielson and G. F. Koster, 'Spectroscopic Coefficients for the p^n, d^n and f^n Configurations', MIT Press, Cambridge, Mass., 1963.
31 C. K. Jørgensen, 'Absorption Spectra and Chemical Bonding in Complexes', Pergamon, London, 1962.
32 J. F. Wyart, V. Kaufman and J. Sugar, *Phys. Scr., 22,* 389 (1980).
33 C. H. H. Van Deurzen, K. Rajnak and J. G. Conway, *J. Opt. Soc, Am., B1,* 45 (1984).
34 S. Hubert, P. Delamoye, S. Lefrant, M. Lepostollec and M. Hussonnois, *J. Solid State Chem., 36,* 36 (1981).
35 L. Bernard, R. Currat, P. Delamoye, C. M. E. Zeyen, S. Hubert and R. de Kouchkovsky, *J. Phys. C, 16,* 433 (1983).
36 P. Delamoye and R. Currat, *J. Phys. Lett., 43,* 655 (1982).
37 P. Delamoye, J. C. Krupa, J. G. Conway and N. Edelstein, *Phys. Rev. B, 28,* 4913 (1983).
38 J. C. Krupa, C. Khan Malek, P. Delamoye, B. Moine and C. Pedrini, *Phys. Status Solidi (B), 140,* 289 (1987).
39 F. Auzel, S. Hubert and P. Delamoye, *J. Lumin., 26,* 251 (1982).
40 J. D. Axe, *Ph.D. Thesis,* Univ. California Lawrence Radiation Laboratory, Berkeley, Calif., 1960.
41 N. Edelstein, D. Brown and B. Whittaker, *Inorg. Chem., 13,* 563 (1974).
42 H. D. Amberger, W. Grape and E. Stumpp, *Actinides 1981, Asilomar, Calif.,* Asilomar Conference Abstracts, L.B.L. 12441, 1981.
43 J. C. Krupa, M. Hussonnois, M. Genet and R. Guillaumont, *J. Chem. Phys., 77,* 154 (1982).
44 J. C. Krupa, S. Hubert, M. Foyentin, E. Gamp and N. Edelstein, *J. Chem. Phys., 78,* 2175 (1983).
45 R. C. Naik and J. C. Krupa, *J. Lumin., 31/32,* 222 (1984).
46 P. Delamoye, K. Rajnak, M. Genet and N. Edelstein, *Phys. Rev. B, 28,* 4923 (1983).
47 I. Richman, P. Kisliuk and E. Y. Wong, *Phys. Rev., 155,* 262 (1967).
48 D. J. Mackey, W. A. Runciman and E. R. Vance, *Phys. Rev. B, 11,* 211 (1975).
49 E. R. Vance and D. J. Mackey, *Phys. Rev. B, 18,* 185 (1978).
50 E. R. Vance and D. J. Mackey, *J. Phys. C, 7,* 1898 (1974).
51 E. R. Vance and D. J. Mackey, *J. Phys. C, 8,* 3499 (1975).
52 R. McLaughlin, *J. Chem. Phys., 36,* 2699 (1962).
53 H. G. Hecht and J. B. Gruber, *J. Chem. Phys., 60,* 4872 (1974).
54 D. R. Johnston, R. A. Satten, C. L. Schreiber and E. Y. Wong, *J. Chem. Phys., 44,* 3141 (1966).
55 W. A. Hargreaves, *Phys. Rev. B, 2,* 2273 (1970).
56 R. A. Satten, C. L. Schreiber and E. Y. Wong, *J. Chem. Phys., 42,* 162 (1964).
57 E. R. Bernstein and T. A. Keiderling, *J. Chem. Phys., 59,* 2105 (1973).
58 B. Briat, P. Delamoye, J. C. Rivoal, S. Hubert and P. Evesque, *J. Phys., 46,* 1375 (1985).
59 C. Khan Malek and J. C. Krupa, *J. Chem. Phys., 84,* 6584 (1986).
60 C. Khan Malek, J. C. Krupa, P. Delamoye and M. Genet, *J. Phys., 47,* 1763 (1986).
61 C. Khan Malek, J. C. Krupa and M. Genet, *Spectrochim. Acta, Part A, 42,* 907 (1986).
62 E. Gamp, N. Edelstein, C. Khan Malek, S. Hubert and M. Genet, *J. Chem. Phys., 79,* 2023 (1983).
63 P. Delamoye, J. C. Krupa, S. Kern, C. K. Loong and G. H. Lander, *J. Less-Common Met., 122,* 59 (1986).
64 A. Murasik, J. Leciejewicz and Z. Zolnierek, *Phys. Status Solidi B, 80,* 137 (1977).
65 Z. Zolnierek, Z. Gajek and C. Khan Malek, *Physica B, 125,* 199 (1984).
66 S. Hubert, E. Simoni and M. Genet, *J. Less-Common Met., 122,* 81 (1986).
67 K. Rajnak, E. Gamp, R. Shinomoto and N. Edelstein, *J. Chem. Phys., 80,* 5942 (1984).
68 R. A. Satten, C. L. Schreiber and E. Y. Wong, *J. Chem. Phys., 78,* 79 (1983).
69 F. Auzel and O. Malta, *J. Phys., 44,* 201 (1983).
70 H. D. Amberger and G. R. Sienel, *Z. Naturforsch., Teil B, 31,* 769 (1976).
71 H. D. Amberger, *J. Organomet. Chem., 116,* 219 (1976).
72 H. D. Amberger, R. D. Fischer and K. Yunlu, *Organometallics,* in press.
73 K. K. Sharma and J. O. Artman, *J. Chem. Phys., 50,* 1241 (1969).
74 M. P. Lahalle, J. C. Krupa, R. Guillaumont and C. Rizzoli, *J. Less-Common Met., 122,* 65 (1986).
75 J. G. Conway, *J. Chem. Phys., 41,* 904 (1964).

76 W. C. Waggener, *J. Chem. Phys., 62,* 382 (1958).
77 I. Poirot, W. Kot, G. Shalimoff, N. Edelstein, M. M. Abraham, C. B. Finch and L. Boatner, ms. in preparation.
78 K. Rajnak, R. H. Banks, E. Gamp and N. Edelstein, *J. Chem. Phys., 80,* 12 (1984).
79 E. R. Menzel and J. B. Gruber, *J. Chem. Phys., 54,* 3857 (1971).
80 E. R. Menzel, J. B. Gruber and J. L. Ryan, *J. Chem. Phys., 57,* 4287 (1972).
81 J. B. Gruber and E. R. Menzel, *J. Chem. Phys., 50,* 3772 (1969).
82 L. B. Asprey and R. A. Penneman, *Inorg. Chem., 1,* 134 (1962).
83 B. F. Myasoedov, I. A. Lebedev and V. M. Mikhailov, *Dok. Akad. Nauk SSSR, 211,* 1351 (1973).
84 D. D. Ensor, J. R. Peterson, R. G. Haire and J. P. Young, *J. Inorg. Nucl. Chem., 43,* 1001 (1981).
85 G. M. Jursich, J. V. Beitz, W. T. Carnall, G. L. Goodman, C. W. Williams and L. R. Morss, to be published.
86 L. P. Varga, R. D. Baybarz, M. J. Reisfeld and L. B. Asprey, *J. Inorg. Nucl. Chem., 35,* 2775 (1973).
87 L. P. Varga, R. D. Baybarz, M. J. Reisfeld and J. B. Mann, *J. Inorg. Nucl. Chem., 35,* 2303 (1973).
88 W. T. Carnall and H. M. Crosswhite, in J. J. Katz, G. T. Seaborg and L. R. Morss (eds.), 'The Chemistry of the Actinide Elements', Vol. 2, Chapman and Hall, London, 1986.
89 W. T. Carnall, *J. Less-Common Met., 122,* 1 (1986).
90 R. D. Cowan and D. C. Griffin, *J. Opt. Soc. Am., 66,* 1010 (1976).
91 K. Rajnak, personal communication.
92 C. E. Schaffer and C. K. Jørgensen, *J. Inorg. Nucl. Chem., 8,* 143 (1958).
93 D. J. Newman, *Aust. J. Phys., 30,* 315 (1977).
94 C. Khan Malek, J. C. Krupa and M. Genet, *Inorg. Chim. Acta, 115,* 115 (1986).
95 J. C. Conway, J. C. Krupa, P. Delamoye and M. Genet, *J. Chem. Phys., 74,* 849 (1981).
96 T. Hayhurst, G. Shalimoff, J. G. Conway, N. Edelstein, L. A. Boatner and M. Abraham, *J. Chem. Phys., 76,* 3960 (1982).
97 D. L. Wood, J. Ferguson, K. R. Knox and J. F. Dillon, *J. Chem. Phys., 39,* 890 (1963).
98 P. Delamoye, *Ph.D. Thesis,* Université Paris-Sud, 1985.
99 M. P. Lahalle, *Ph.D. Thesis,* Université Paris-Sud, 1986.
100 C. Khan Malek, *Ph.D. Thesis,* Université Paris-Sud, 1985.